Supporting Information

Colossal Negative Thermal Expansion in a Cucurbit[8]uril-Enabled Uranyl-Organic Polythreading Framework via Thermally induced Relaxation

Qiu-yan Jin,[a,b] Yuan-yuan Liang,[a,b] Zhi-hui Zhang,*[c] Liao Meng,[a] Jun-shan Geng,[a] Kong-qiu Hu,[a] Ji-pan Yu,[a] Zhi-fang Chai,[a] Lei Mei,*[a] and Wei-qun Shi *[a]

[a.] *Laboratory of Nuclear Energy Chemistry, Institute of High Energy Physics, Chinese Academy of Sciences, Beijing 100049, China.*

E-mail: meil@ihep.ac.cn; shiwq@ihep.ac.cn

[b.] *University of Chinese Academy of Sciences, Beijing 100049, China.*

[c.] *Jiangsu Key Laboratory of Advanced Catalytic Materials and Technology, Advanced Catalysis and Green Manufacturing Collaborative Innovation Center. Changzhou University, Changzhou 213164, China. zhangzh@cczu.edu.cn*

Contents

1. Supplementary Methods

Materials and characterization methods

Caution! Depleted uranium used here in the form of uranyl nitrate hexahydrate, $UO_2(NO_3)_2 \cdot 6H_2O$, possesses chemical and radioactive toxicity, and should be handled according to standard precautions and procedures. A stock solution of uranyl ion (0.5 M) was prepared by dissolving certain amounts of $UO_2(NO_3)_2 \cdot 6H_2O$ in deionized water before the hydrothermal synthesis. All other reagents were purchased commercially and used as received.

^1H NMR were carried out on a Bruker AVANCE III (500 MHz, Bruker, Switzerland) with deuterium oxide as a solvent. ESI-MS spectra were obtained with a Bruker AmaZon SL ion trap mass spectrometer (Bruker, USA). Powder XRD measurements were recorded on a Bruker D8 Advance diffractometer with Cu Kα radiation (λ=1.5406 Å) in the range of 5-50° (step size: 0.02º). Thermogravimetric analysis (TGA) employed a TA Q500 analyzer over the temperature range of room temperature and 800 °C in air atmosphere with a heating rate of 5 °C/min. Differential Scanning Calorimeter (DSC) experiments were conducted on a TA Q2000 analyzer over the temperature range of -50~40 °C (corresponding to 223.15~313.13 K) in nitrogen atmosphere with a heating and cooling rate of 5 °C/min. Fourier transform infrared (IR) spectra were recorded from KBr pellets in the range of 4000-400 cm^{-1} on a Bruker Tensor 27 spectrometer.

Synthesis of 1-(4-carboxybenzyl)-4,4'-bipyridinium chloride ([Hbcbpy]Cl)

4,4'-Bipyridine (4.68 g, 30 mmol) and 4-chloromethylbenzoic acid (3.41 g, 20 mmol) were dissolved in 100 mL of acetonitrile and heated to reflux at 85 ºC for 48 h. The precipitate was filtered after cooling to room temperature, rinsed with acetonitrile and dried at 60 ºC for 24 h to give the product (6.06 g, 92.7%). ^1H NMR (500 MHz, D_2O), δ (ppm) = 9.05 (2H, d, pyridinium H), 8.83 (2H, d, pyridinium H), 8.43 (2H, d, pyridine H), 8.10 (2H, d, pyridine H), 7.97 (2H, d, phenyl H), 7.52 (2H, d, phenyl H), 5.92 (2H, s, CH_2). ESI-MS (Da): calculated for $[C_{18}H_{15}N_2O_2]^+$, 291.11; found, 291.20 ($[M]^+$).

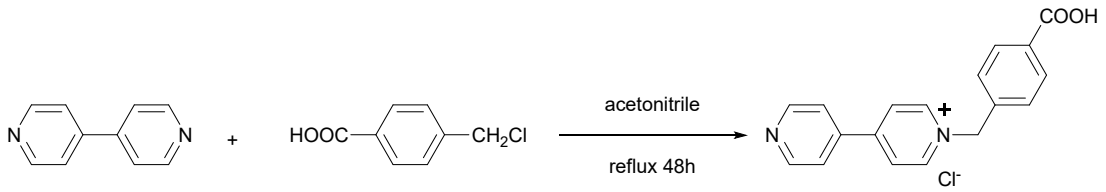

Scheme S1. Synthetic route of [Hbcbpy]Cl.

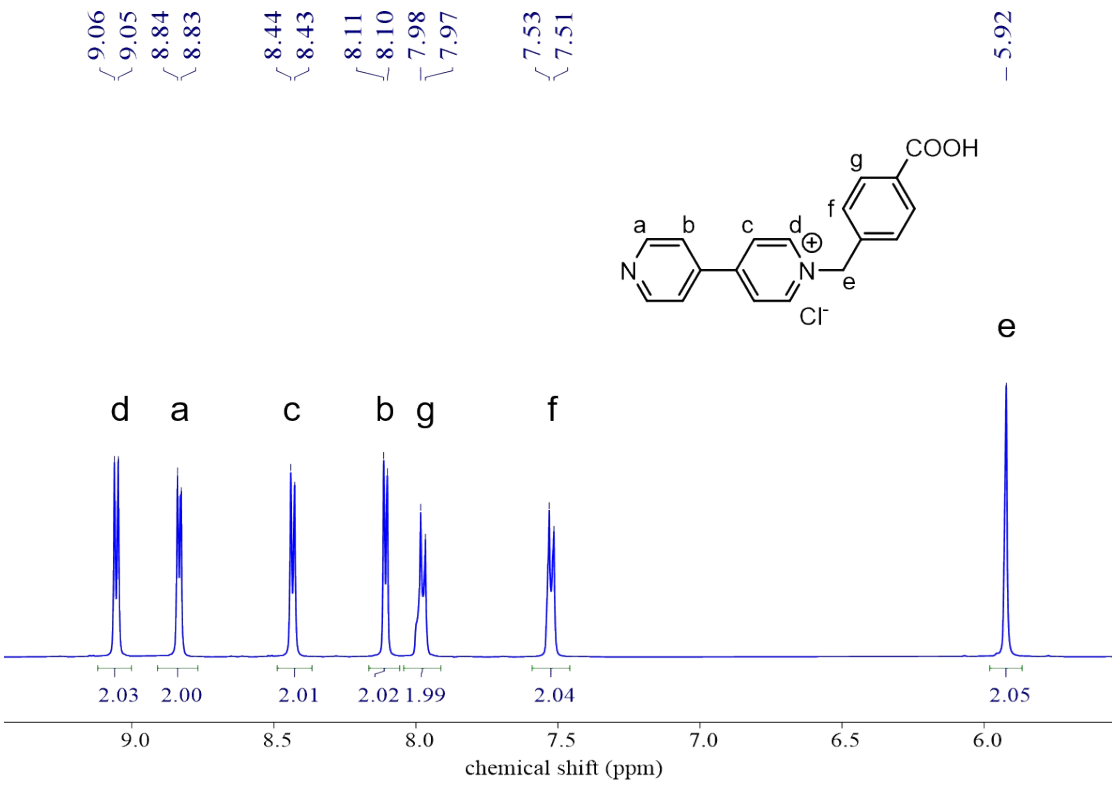

Fig. S1 ^{1}H NMR of [Hbcbpy]Cl in D_2O (500 MHz).

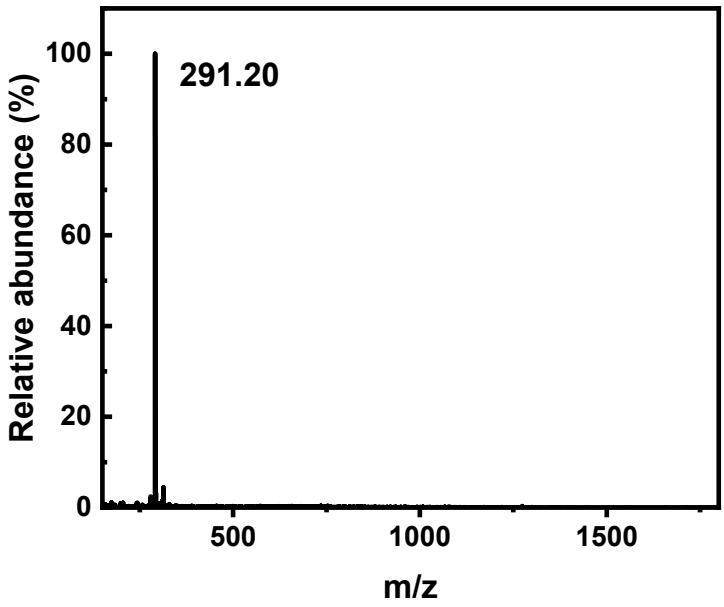

Fig. S2 ESI-MS spectrum of [Hbcbpy]Cl in H_2O.

Synthesis of cucurbit[8]uril (CB8)

CB8 was synthesized according to the literature[1] with minor modification. Glycoluril (28.4 g) was dissolved in 150 mL of concentrated hydrochloric acid followed by adding 12 g of paraformaldehyde and heated to reflux at 100 ºC for 12h. After cooling to room temperature, the reaction mixture was concentrated using rotary evaporation until a small

amount of precipitation appeared, and added to a large amount of acetone to give the precipitation. Washed with a large amount of deionized water and stirred overnight until it was no longer dissolved, the precipitation was then filtered and dissolved with 4M hydrochloric acid (120 mL) overnight with the aid of stirring to remove cucurbit[6]uril. The white solid was filtered, washed with 50% formic acid (30 mL), and then washed with a large amount of deionized water. The solid was filtered and dried at 60 ºC for 24h to obtain 1.9 g of CB8, yield: 4.75%. ^{1}H NMR (500 MHz, D_2O), δ (ppm) = 5.80 (16H, d, one of CH_2 pointing out of the CB8 cavity), 5.54 (16H, s, CH), 4.21 (16H, d, one of CH_2 pointing towards the CB8 cavity).

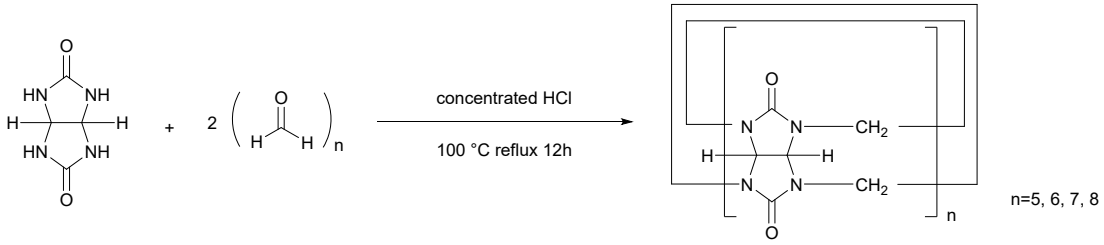

Scheme S2. Synthetic route of CB8.

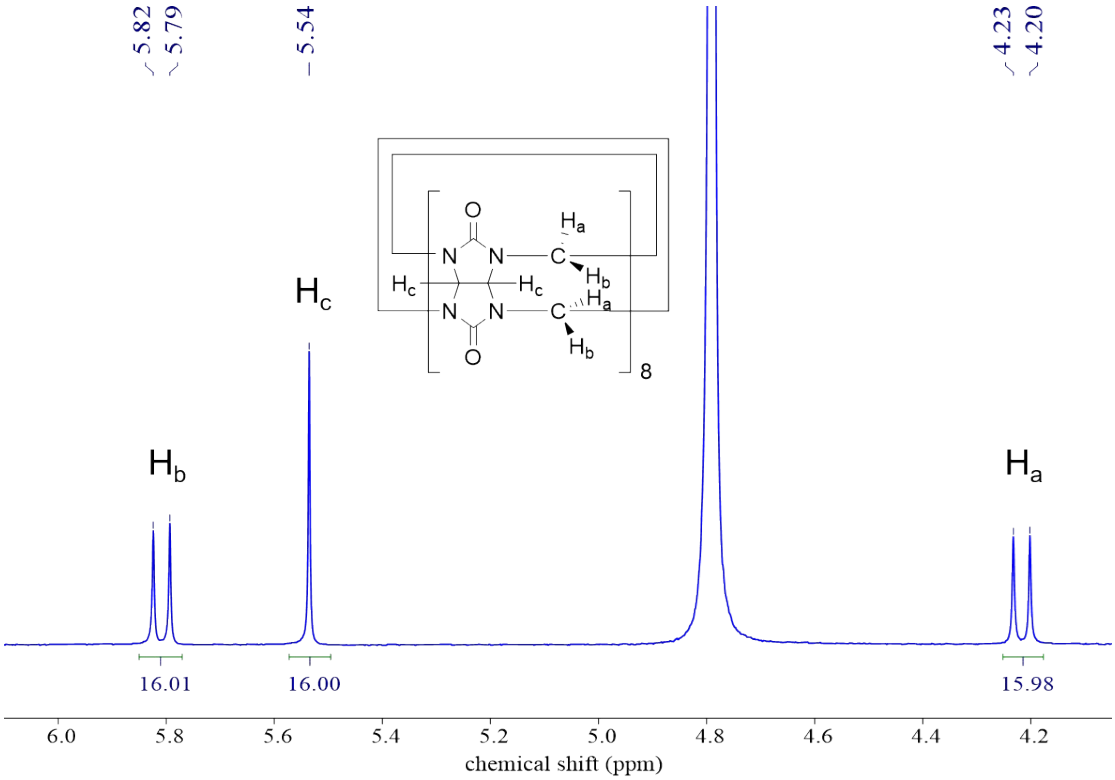

Fig. S3 ^{1}H NMR of cucurbit[8]uril (CB8) in D_2O (500 MHz).

Synthesis of [(Hbcbpy)$_2$@CB8]Cl$_2$

[Hbcbpy]Cl (32.8 mg, 0.1 mmol), CB8 (66.4 mg, 0.05 mmol) and 2 mL deionized water were added into a 10 mL Teflon autoclave. The initial pH of the reaction mixture was 2.40. The autoclaved was then sealed with a stainless-steel kettle jacket and heated at 150 ºC for 48h. After naturally cooling to room temperature, the pH of the solution was measured to be 2.33. Tandem mass spectrometry (MS_n) experiments (Fig. S4) and ^{1}H-NMR spectra

(Fig. S5) were used to analyse the resultant crystals. A m/z peak of 955.85 corresponding to the $[2(Hbcbpy)+CB8]^{2+}$ species was observed, which was subjected to MS-MS analyse through collision induced dissociation to give fragment peaks of $[Hbcbpy]^{+}$ (m/z = 291.20) and $([Hbcbpy]+CB8)^{+}$ (m/z = 1619.64) as decomposition products. Moreover, suitable single crystals were picked out for single-crystal X-ray structure determination (Fig. S6).

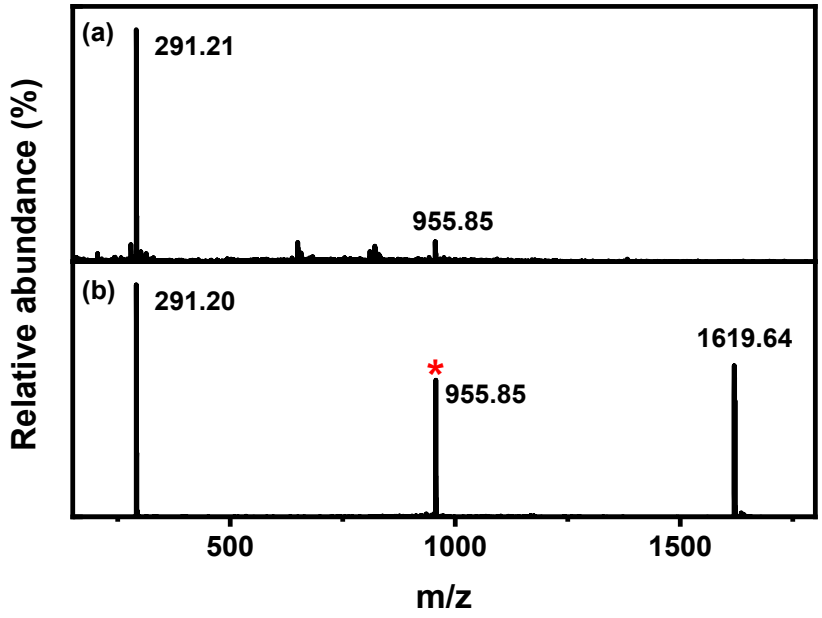

Fig. S4 ESI-MS analyses of crystals of $([Hbcbpy]Cl)_2$@CB8: (a) original result of dissolved crystals ($[Hbcbpy]^{+}$, m/z = 291.21; $[2(Hbcbpy)+CB8]^{2+}$, m/z = 955.85); (b) MS-MS result of the selected peak of 955.85 corresponding to the $[2(Hbcbpy)+CB8]^{2+}$ species (($[Hbcbpy]^{+}$, m/z = 291.20; $[2(Hbcbpy)+CB8]^{2+}$, m/z = 955.85; $([Hbcbpy]+CB8)^{+}$, m/z = 1619.64).

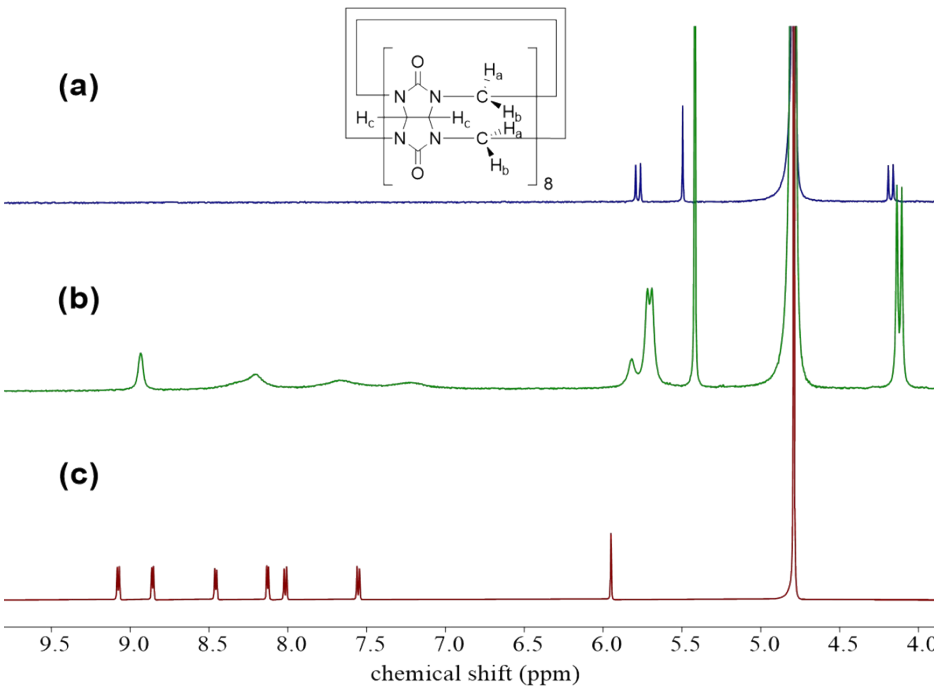

Fig. S5 ^{1}H NMR spectra (500 MHz, D_2O, 298 K): (a) CB8, (b) $([Hbcbpy]_2@CB8)Cl_2$ crystals dissolved in D_2O and (c) [Hbcbpy]Cl.

Single-crystal X-ray diffraction measurements

All crystal data were collected using a Bruker D8 VENTURE X-ray diffractometer with a Mo Kα X-ray source (λ = 0.71073 Å). Data frames were collected using the program APEX 3 and processed using the program SAINT routine in APEX 3. All crystal structures were solved by means of direct methods (SHELXL-97[2]) and refined with full-matrix least squares on SHELXL-2014[3] based on Olex2 software package.[4] The diffraction contribution of disordered solvent molecules was calculated by using a solvent-masking procedure as implemented in Olex2. All non-hydrogen atoms were refined with anisotropic displacement parameters. The carbon-bound hydrogen atoms were placed at calculated positions, and all hydrogen atoms were treated as riding atoms with an isotropic displacement parameter equal to 1.2 times that of the parent atom.

Cycle experiment of thermal responsive behaviour

In cycle test of thermal responsive behaviour, the crystal unit cell data was obtained by fast scan mode of single-crystal X-ray diffraction, which started at 170 K. A series of temperature points within the range of 170 K-320 K were set according to the experimental requirements: first heating protocol, 170 K-320 K (170 K, 200 K, 240 K, 250 K, 260 K, 270 K, 280 K, 290 K, 300 K, 310 K and 320 K); a following reverse cooling protocol, 320-240 K (320 K, 310 K , 300 K, 290 K, 280 K, 270 K, 260 K, 250 K and 240 K); a second heating protocol, 240 K-320 K (240 K, 250 K, 260 K, 270 K, 280 K, 290 K, 300 K, 310 K and 320 K). The experiment started at 170 K, and gradually raised the temperature to the temperature points set in sequence. After heating to the target temperature with a heating rate of 120 K h^{-1}, the crystal was kept at target temperature for 10 min before subject to subsequent measurement.

2. Supplementary Figures

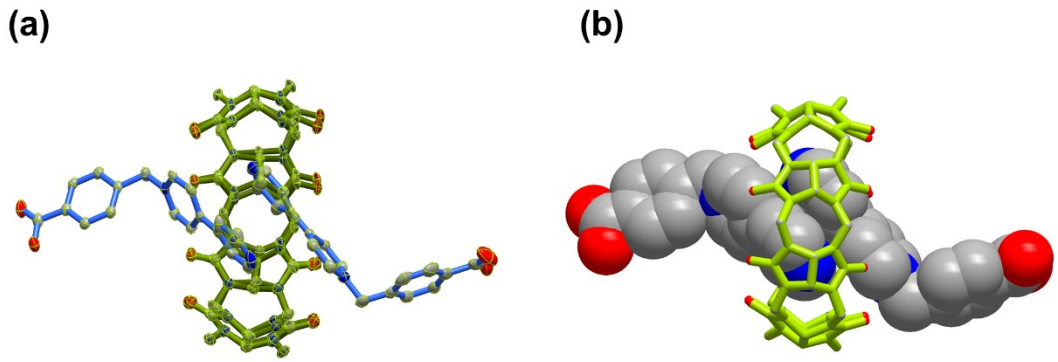

Fig. S6 Crystal structure of $([Hbcbpy]Cl)_2$@CB8 (hydrogen atoms are omitted for clarity): (a) ORTEP drawing of the asymmetric unit with thermal ellipsoids at 50% probability; (b) space-filling mode showing the inclusion of bipyridine groups in the cavity of CB8 macrocycle.

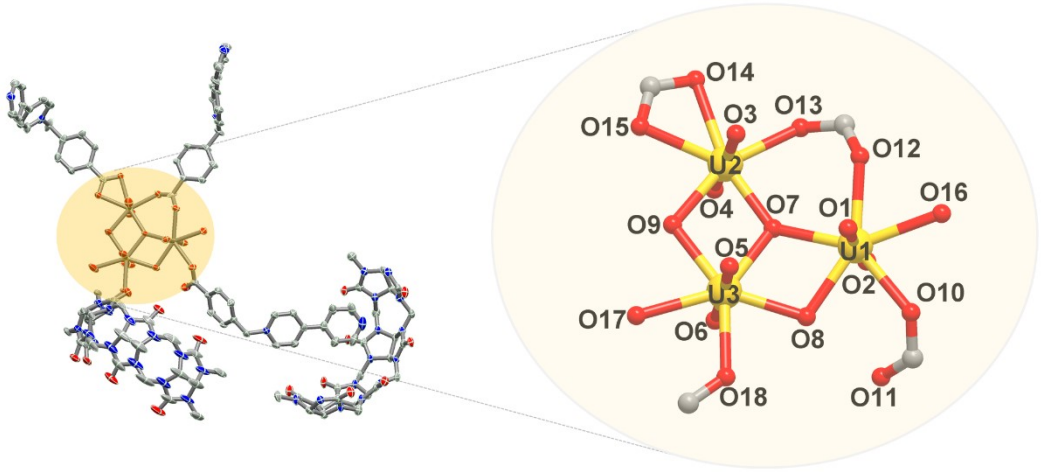

Fig. S7 Crystal structure of $U_3(bcbpy)_3(CB8)$ collected at 170 K (left, the asymmetric unit containing a trimeric uranyl unit, three bcbpy motifs and two halves of CB8 macrocycles; right, enlarged diagram showing the coordination spheres of three uranium centres in the trimeric uranyl unit).

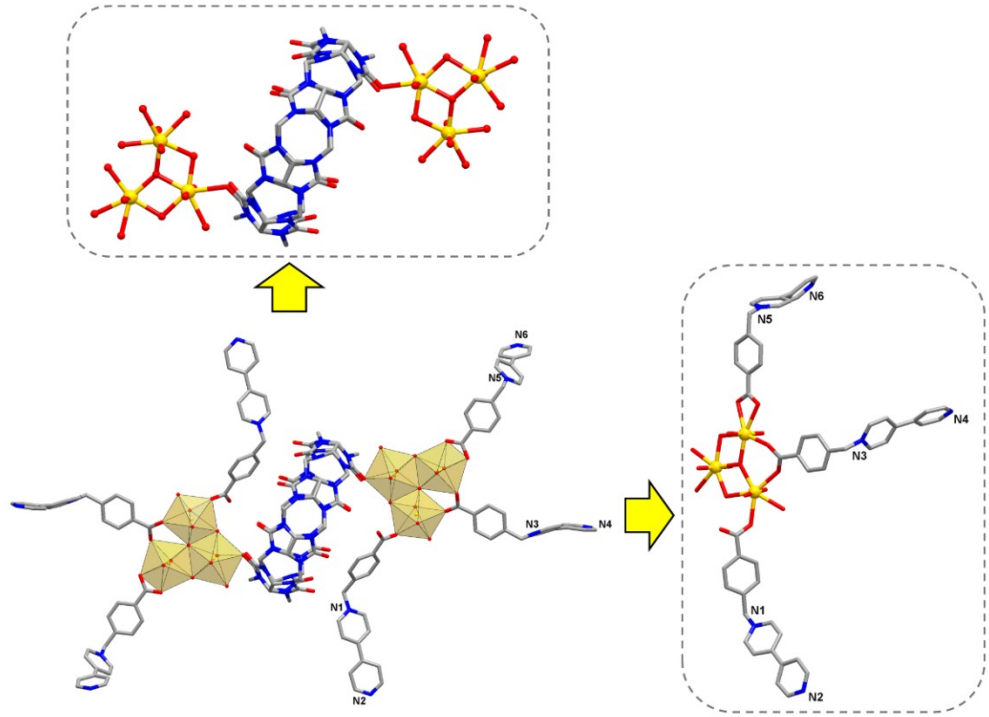

Fig. S8 CB8-bridged hexanuclear unit with six bipyridinium 'arms' hanging outside in $U_3(bcbpy)_3(CB8)$.

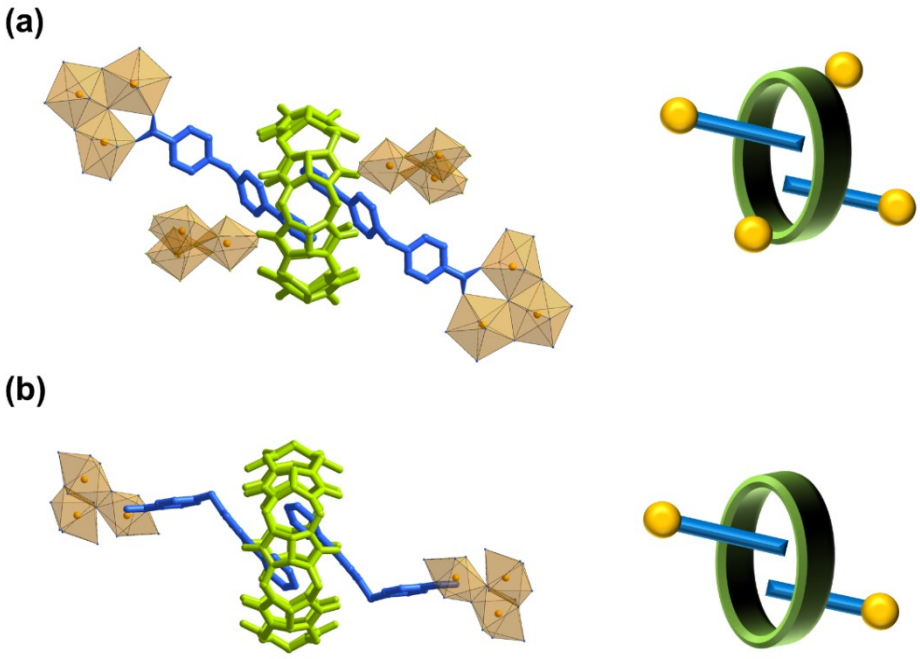

Fig. S9 Two kinds of CB8 macrocycle molecules found in crystal structure of $U_3(bcbpy)_3(CB8)$: (a) CB8 that is coordinated with uranyl but retains the ability to include guests; (b) non-coordinated CB8.

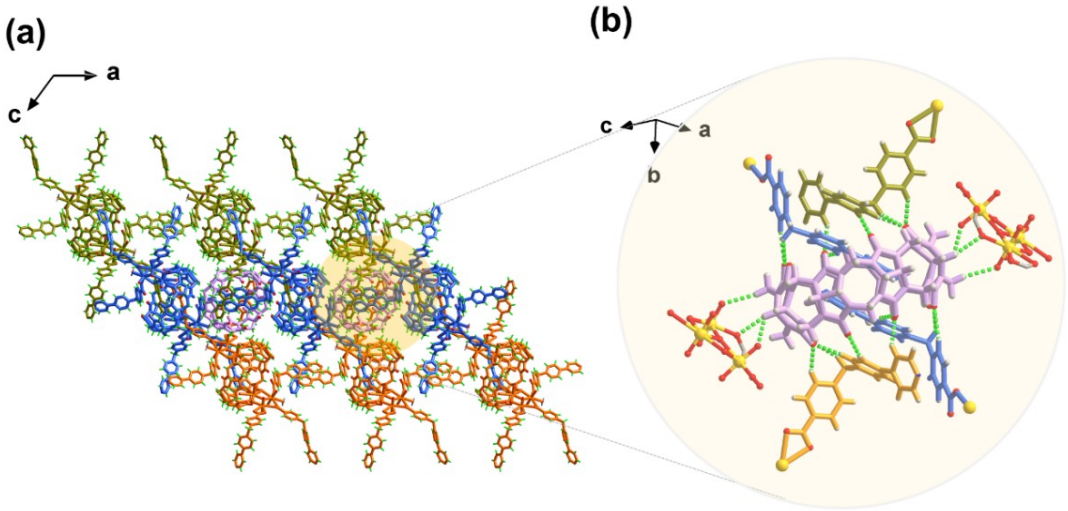

Fig. S10 Intensive hydrogen bond networks around interlayered non-coordinated CB8: (a) location of interlayered non-coordinated CB8; (b) enlarged diagram showing the hydrogen bond networks around a non-coordinated CB8 molecule as well as a pair of encapsulated bcbpy guests (O28···H51(C51), 2.371(4) Å; O29···H46(C46), 2.253(4) Å; O30···H45(C45), 2.350(6) Å; O30···H40(C40), 2.754(3) Å; O31···H40(C40), 2.639(3) Å; O28···H12(C12), 2.668(5) Å; O28···H13(C13), 2.665(4) Å; O27···H8A(C8), 2.466(3) Å; O27···H6 (C6), 2.535(4) Å; O4···H10C(C102), 2.756(7) Å; O13···H81(C81), 2.484(5) Å; O2···H10B(C101), 2.670(4) Å; O2···H98(C98), 2.328(4) Å).

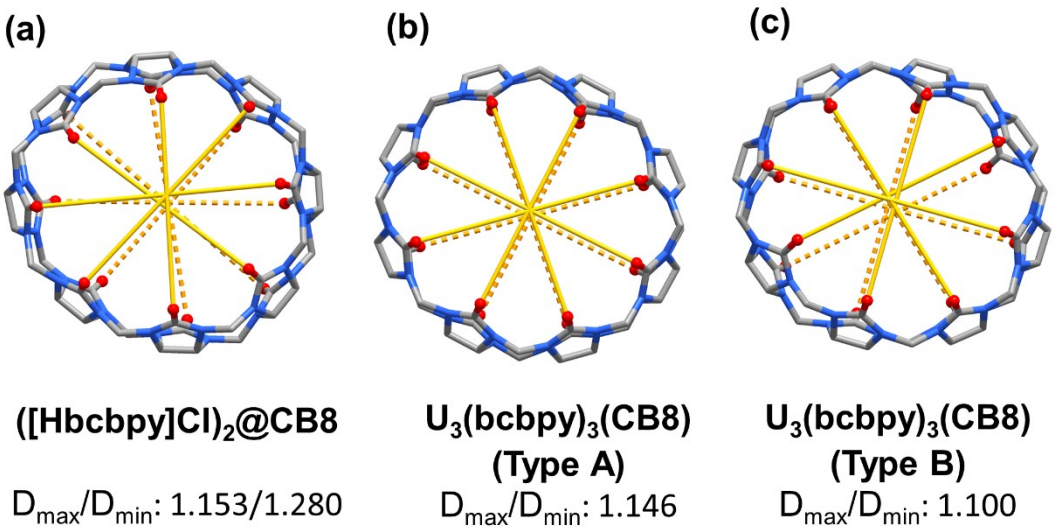

Fig. S11 Molecular structures of macrocyclic CB8 in $([Hbcbpy]Cl)_2$@CB8 and $U_3(bcbpy)_3(CB8)$ with minor variation in molecular conformation.

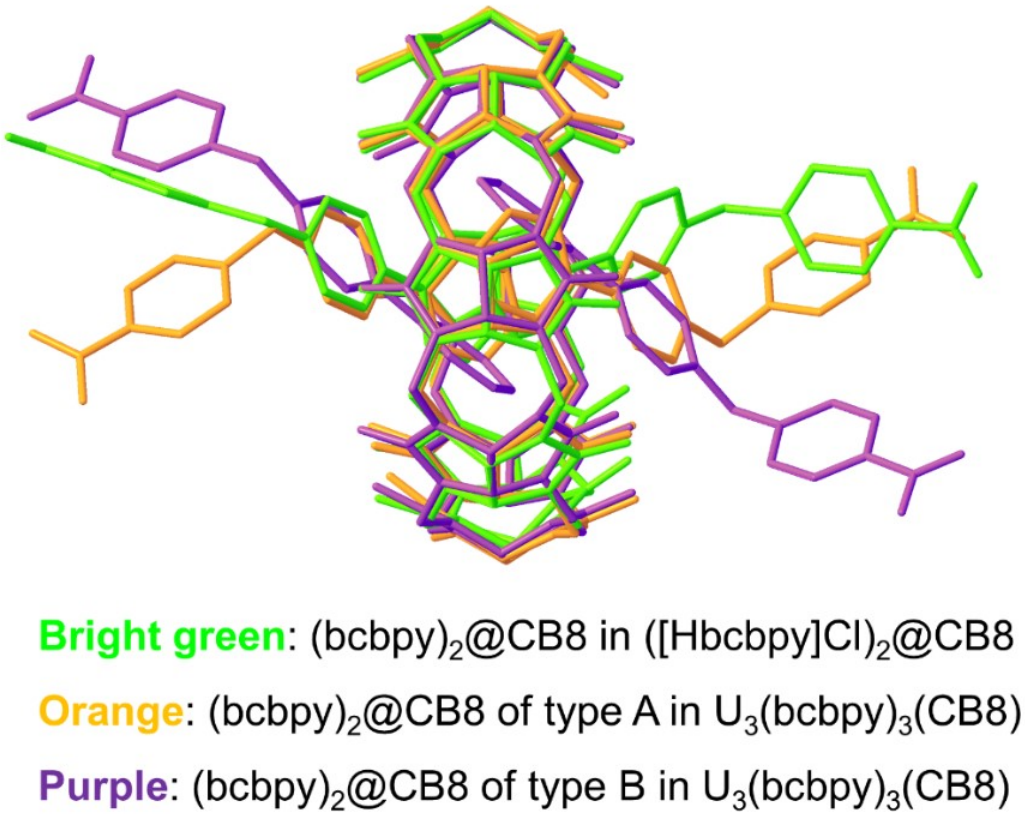

Fig. S12 The bcbpy molecules exhibit intriguing structural dynamics in $([Hbcbpy]Cl)_2$@CB8 and $U_3(bcbpy)_3(CB8)$, among which the methylene phenyl group can be flexibly rotated around the bipyridine group encapsulated in CB8 cavity.

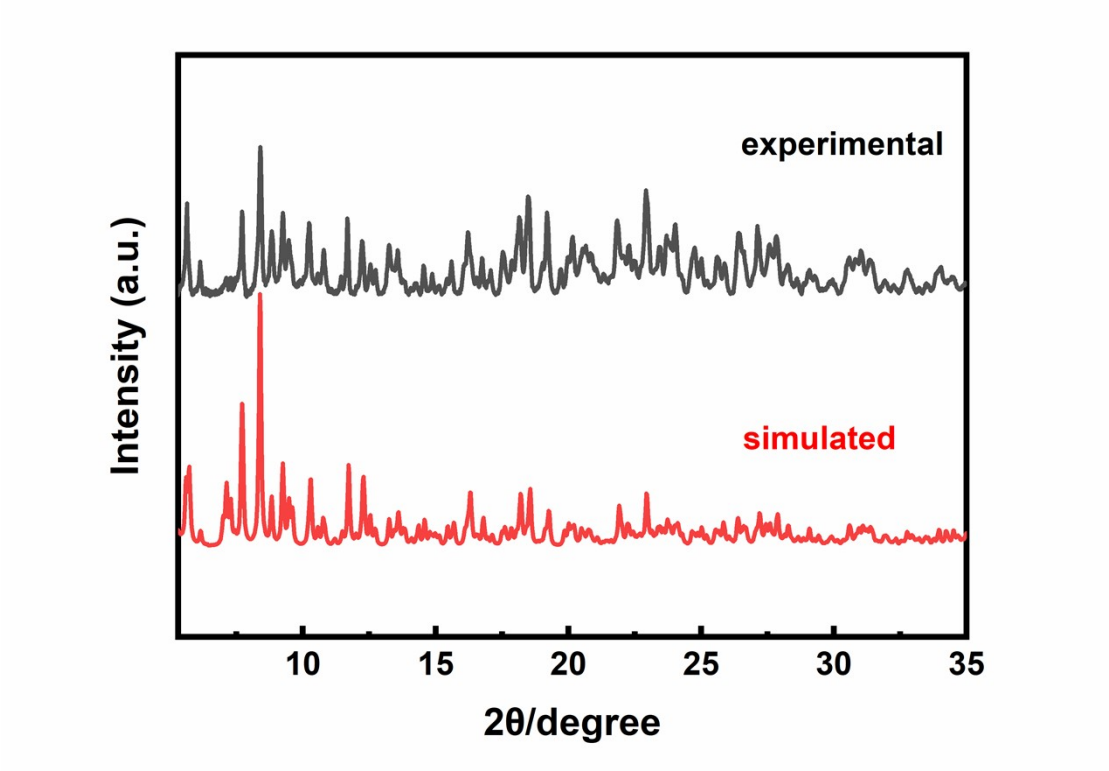

Fig. S13 The powder X-ray diffraction (PXRD) pattern of $U_3(bcbpy)_3(CB8)$.

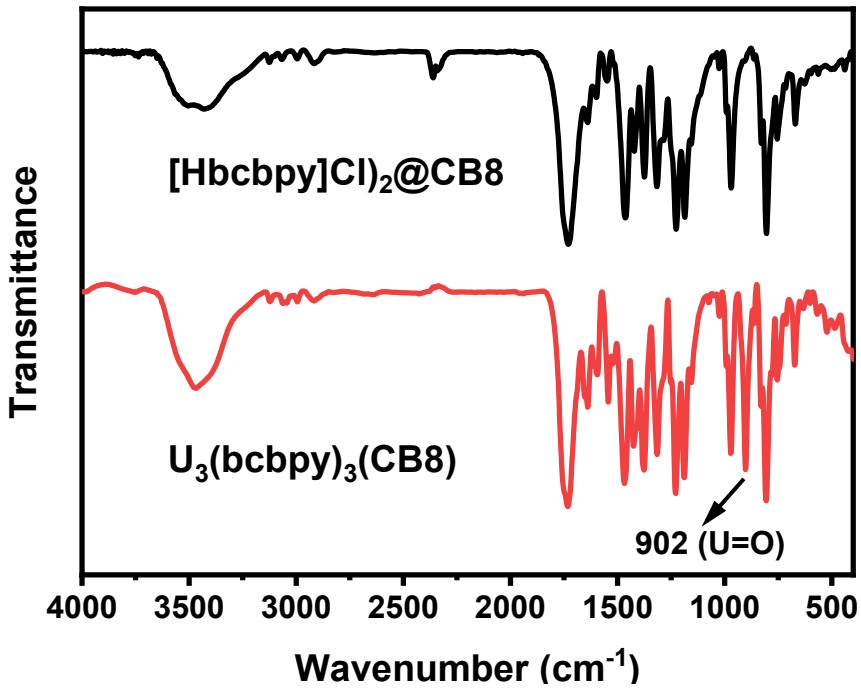

Fig. S14 The Fourier transform infrared (IR) spectra of of $([Hbcbpy]Cl)_2@CB8$ and $U_3(bcbpy)_3(CB8)$ and recorded in the range of 4000-400 cm^{-1}.

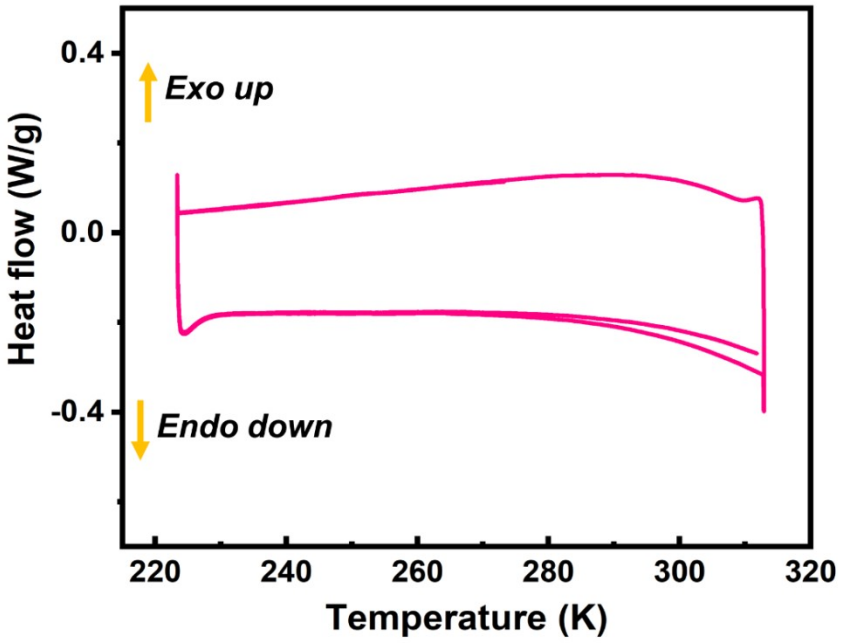

Fig. S15 The differential scanning calorimeter (DSC) result of $U_3(bcbpy)_3(CB8)$ over the temperature range of -50~40 °C (corresponding to 223.15~313.15 K) in nitrogen atmosphere with a heating and cooling rate of 5 °C/min.

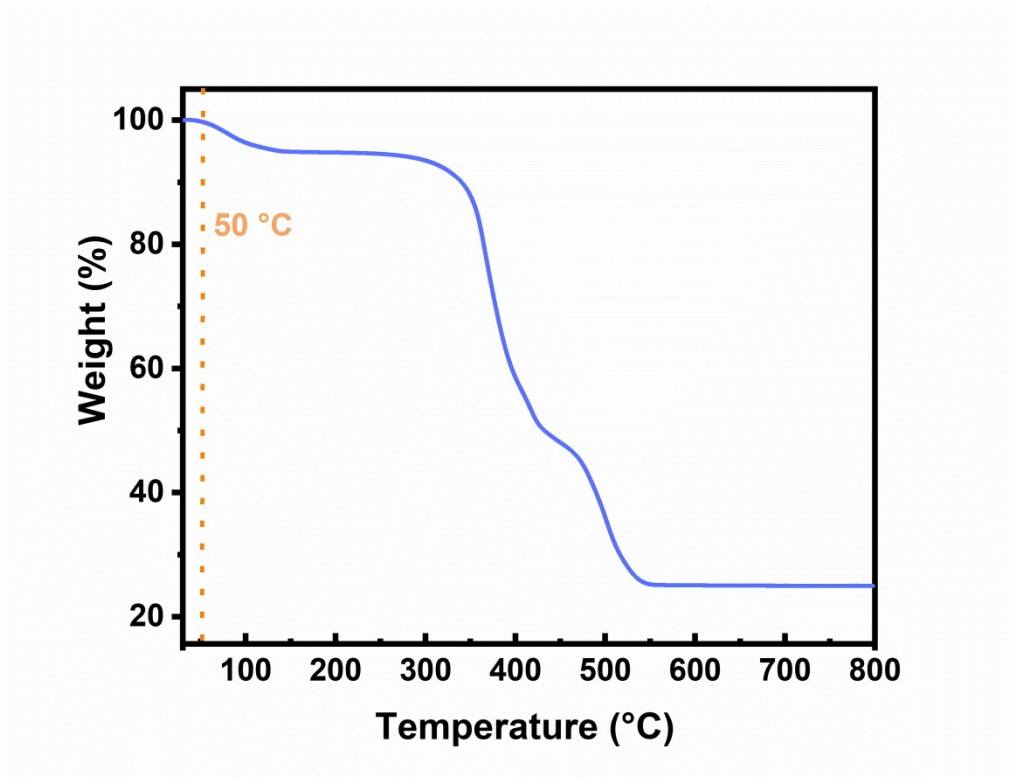

Fig. S16 The thermogravimetric analysis (TGA) result of $U_3(bcbpy)_3(CB8)$ over the temperature range of room temperature and 800 °C in air atmosphere with a heating rate of 5 °C/min, where the loss of water began over 50 °C.

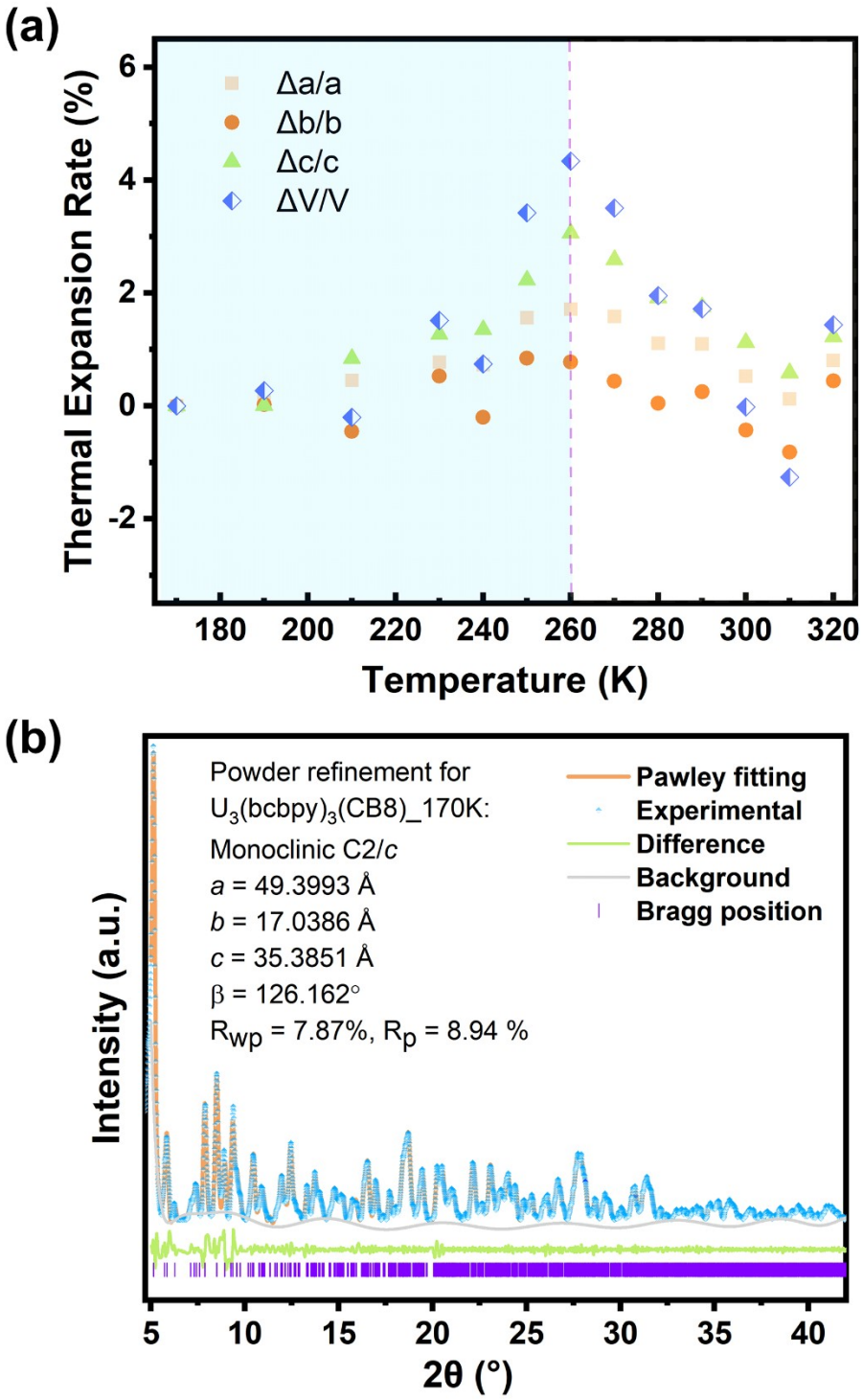

Fig. S17 Temperature-related lattice parameters from profile fitting (using the Pawley method) of the experimental VT-PXRD data of $U_3(bcbpy)_3(CB8)$: (a) lattice parameters in the range of 170 K to 320 K; (b) Pawley refinement of PXRD pattern for $U_3(bcbpy)_3(CB8)$ using the data at 170 K as an example, including Pawley fitting data (organge line), experimental data (blue marks) with background subtracted (grey line), difference

between experimental and calculated data (green line), and the predicted Bragg positions (purple tick marks).

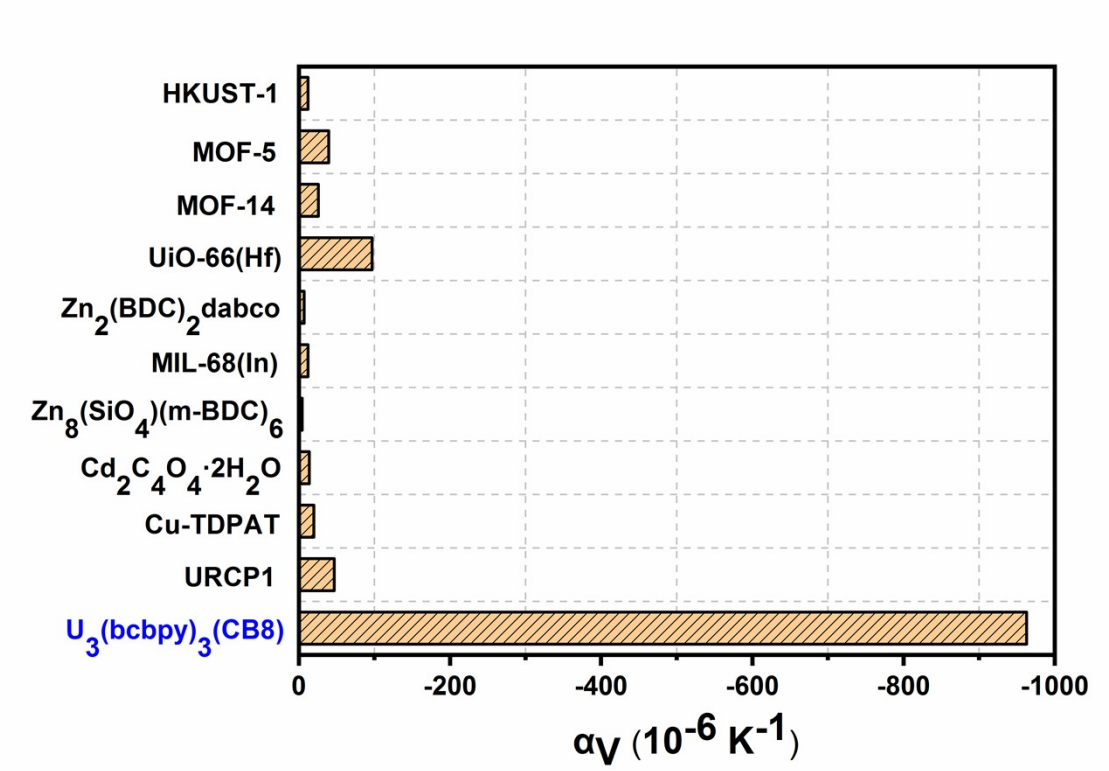

Fig. S18 A comparison of α_V between MOFs and metal-organic rotaxane compounds bearing volumeric NTE reported so far with that of $U_3(bcbpy)_3(CB8)$ here.

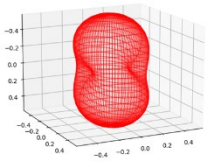

170-260 K

		Component along the crystallographic axes			
Principal axis	α (MK^{-1})	a	b	c	Approximate axis
X_1	21 ± 5	-0.2831	0	-0.9591	[103]
X_2	44 ± 6	0	1	0	[010]
X_3	75 ± 4	-0.9456	0	-0.3253	[301]
V	146 ± 13				

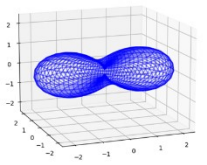

260-300 K

		Component along the crystallographic axes			
Axes	α (MK^{-1})	a	b	c	Approximate axis
X_1	-703 ± 73	0.3714	0	0.9285	[103]
X_2	-276 ± 18	-0.9961	0	-0.0879	[100]
X_3	-27 ± 6	0	1	0	[010]
V	-1055 ± 95				

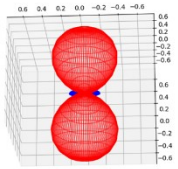

300-330 K

300-330K		Component along the crystallographic axes			
Axes	A (MK^{-1})	a	b	c	Approximate axis
X_1	-61 ± 14	0	1	0	[010]
X_2	8 ± 13	0.2240	0	-0.9746	[103]
X_3	330 ± 50	-0.6813	0	-0.7320	[101]
V	287 ± 24				

Fig. S19 Expansivity indicatrices and fitted thermal expansion coefficients of $U_3(bcbpy)_3(CB8)$ within different temperature ranges calculated using the PASCal software.[5]

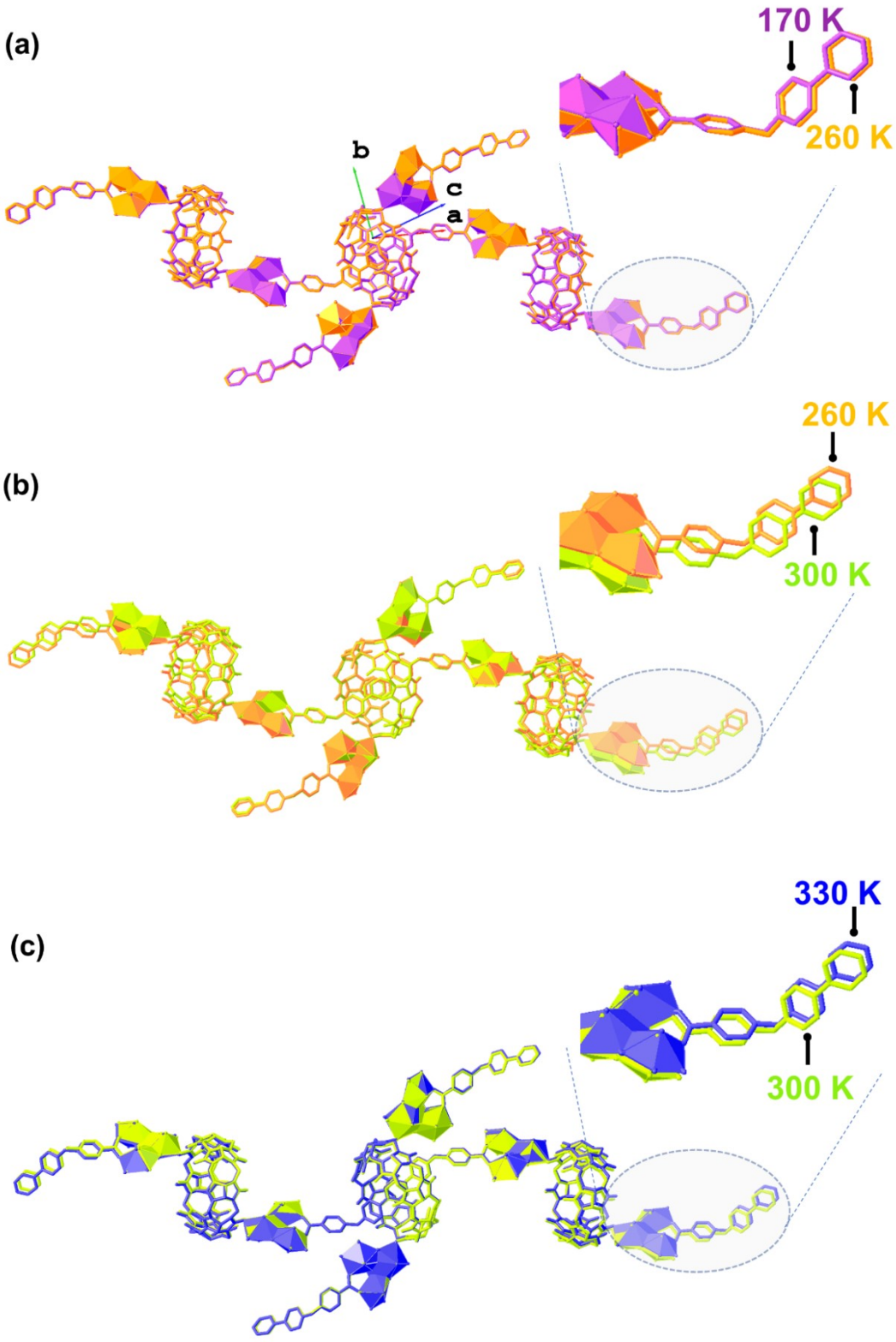

Fig. S20 The overlaid structures of interwined hexanuclear uranyl units on $(10\bar{1})$ plane that extend along [101] axis within the temperature of 170-330 K: (a) direct comparison 170 K and 260 K; (b) direct comparison 260 K and 300 K; (c) direct comparison 300 K and 330 K.

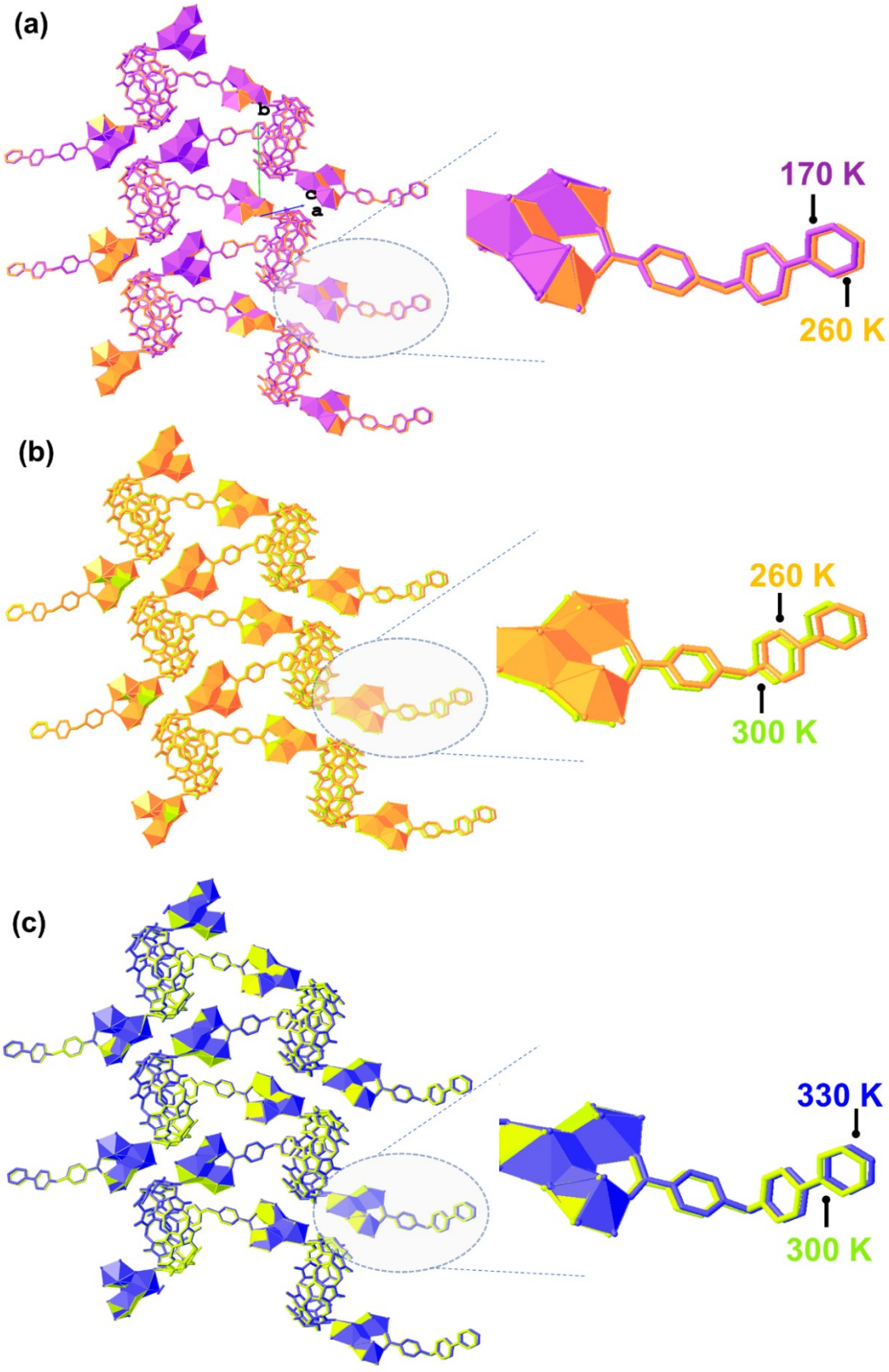

Fig. S21 The overlaid structures of interwined hexanuclear uranyl units on $(10\bar{1})$ plane that extend along *b*-axis (i.e. [010] axis) and [101] axis within the temperature of 170-330 K: (a) direct comparison 170 K and 260 K; (b) direct comparison 260 K and 300 K; (c) direct comparison 300 K and 330 K.

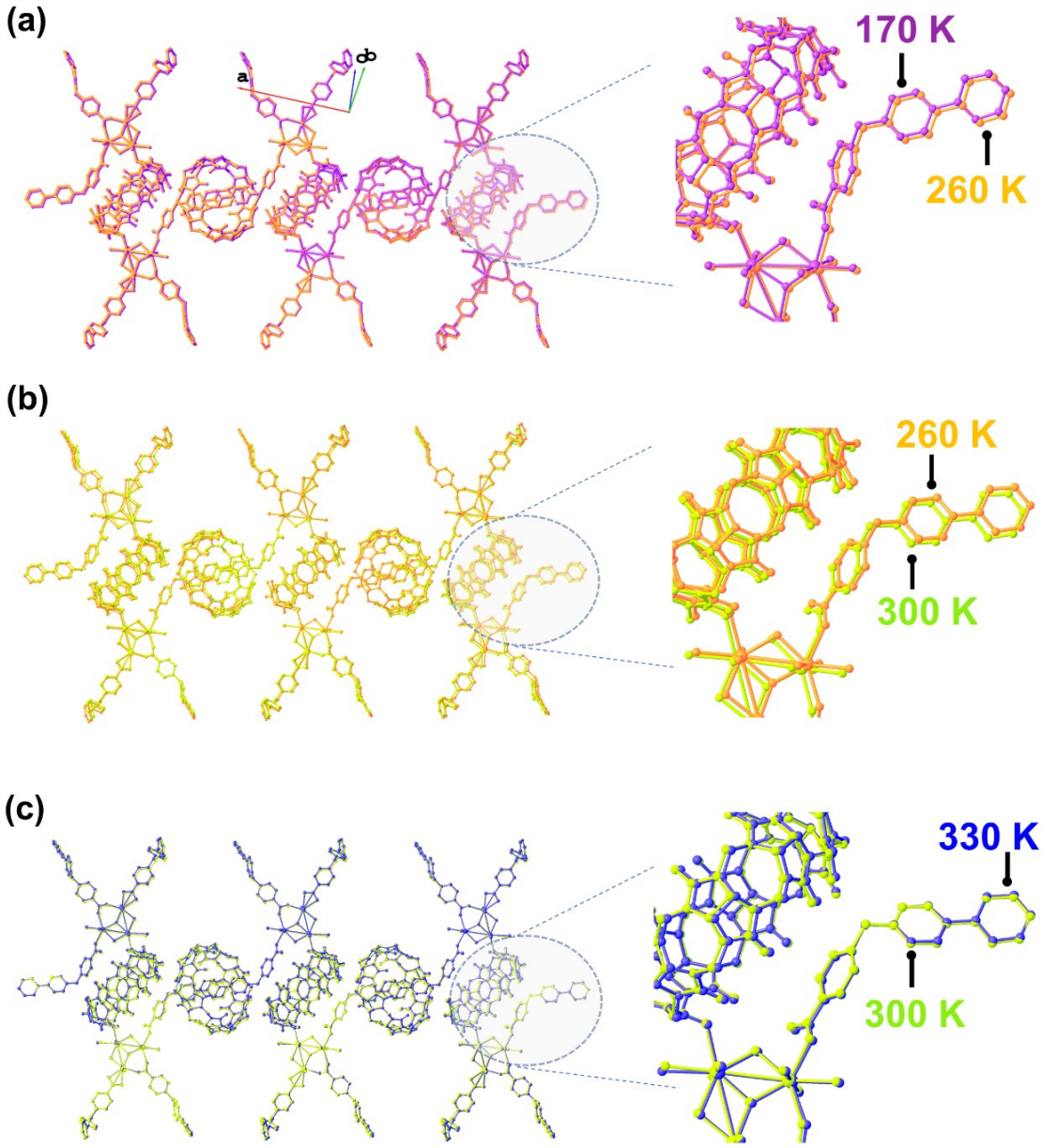

Fig. S22 The overlaid structures of interwined hexanuclear uranyl units on (001) plane that extend along *a*-axis (i.e. [100] axis) within the temperature of 170-330 K: (a) direct comparison 170 K and 260 K; (b) direct comparison 260 K and 300 K; (c) direct comparison 300 K and 330 K.

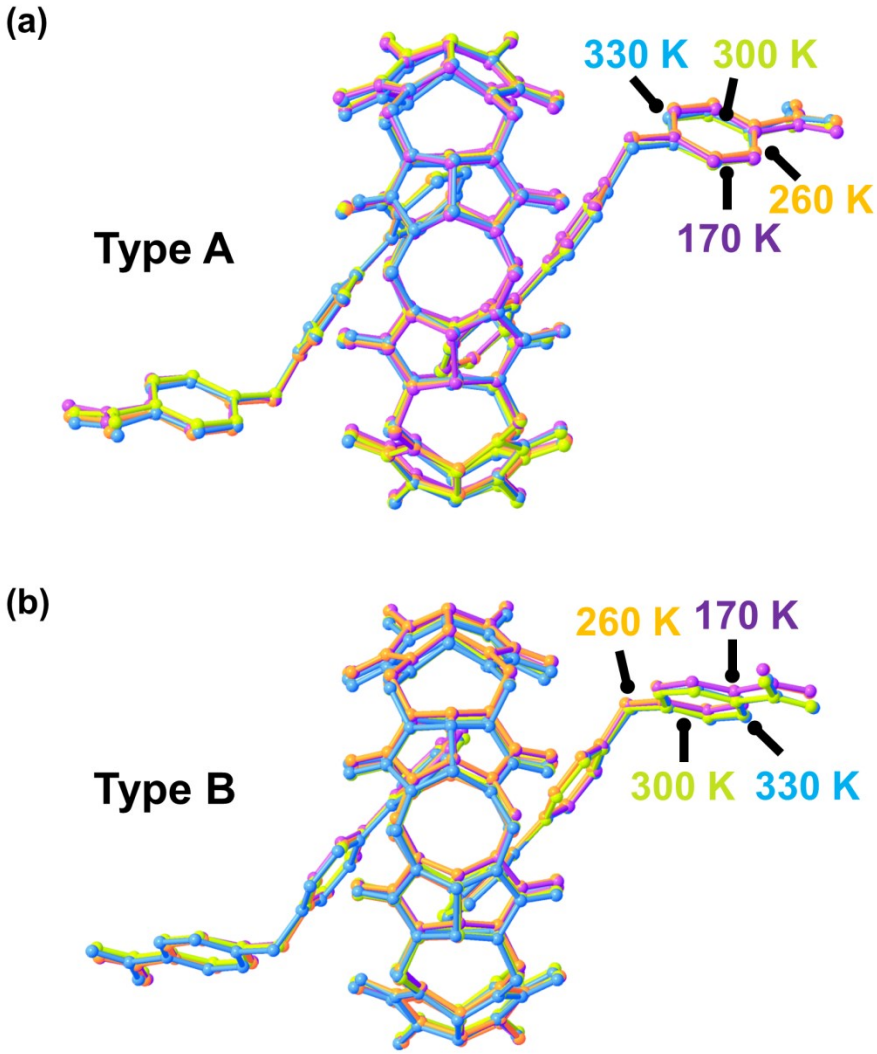

Fig. S23 The overlaid structures of the CB8-based host-guest complex, $(bcbpy)_2$@CB8, within the temperature of 170-330 K: (a) $(bcbpy)_2$@CB8 of type A; (b) $(bcbpy)_2$@CB8 of type B.

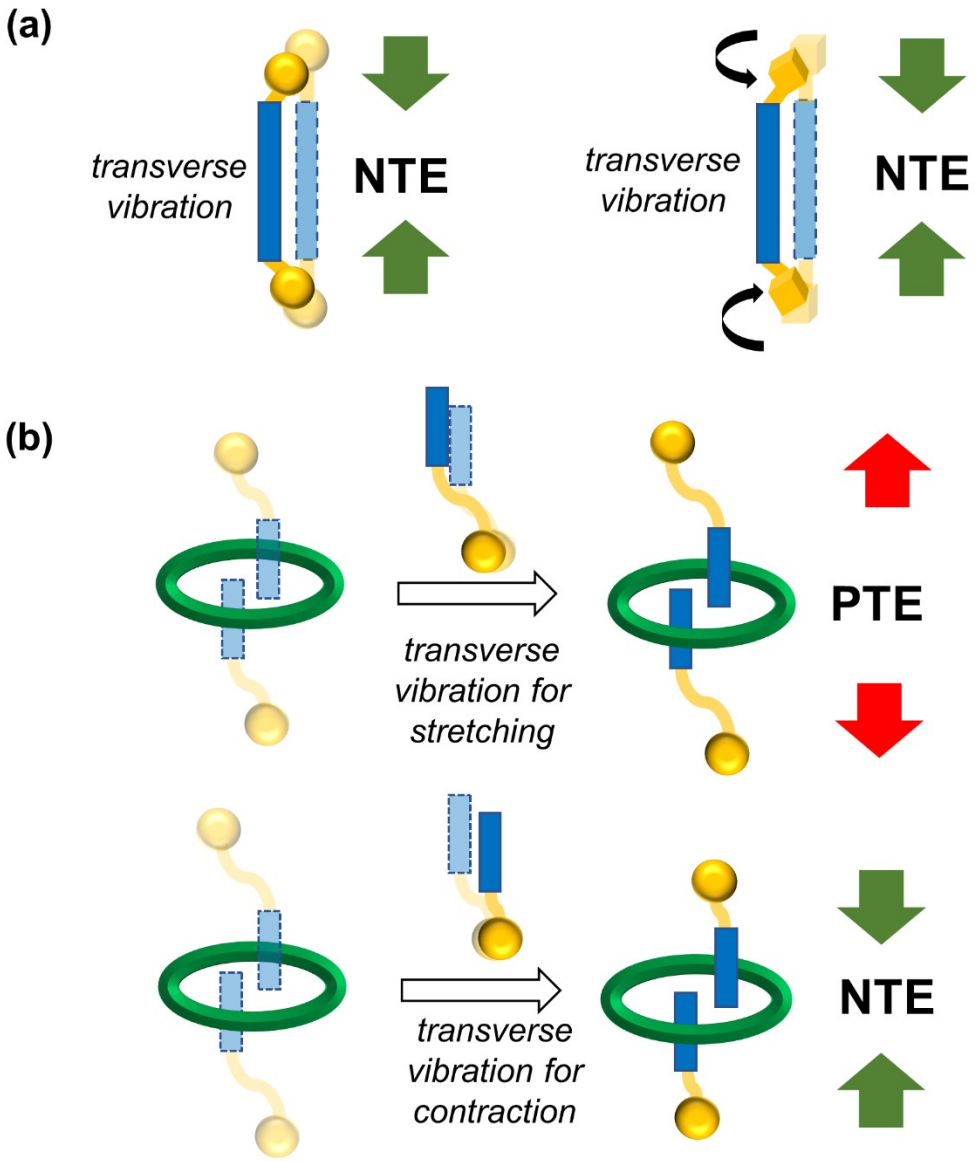

Fig. S24 Relationship between transverse motion of organic or pesudorotaxane linkers and thermal expansion in different types of framework structure materials: (a) typical MOF materials with covalently-bonded organic linkers which shows NTE due to transverse motion of organic linkers; (b) the polythreading framework in this work that can show PTE or NTE due to transverse motion of organic linkers, depending on the moving direction of flexible structs encapsulated in the cavity of CB8 (green cycles: CB8 macrocycles; yellow balls: metal nodes; blue blocks: organic linkers or flexible structs for CB8).

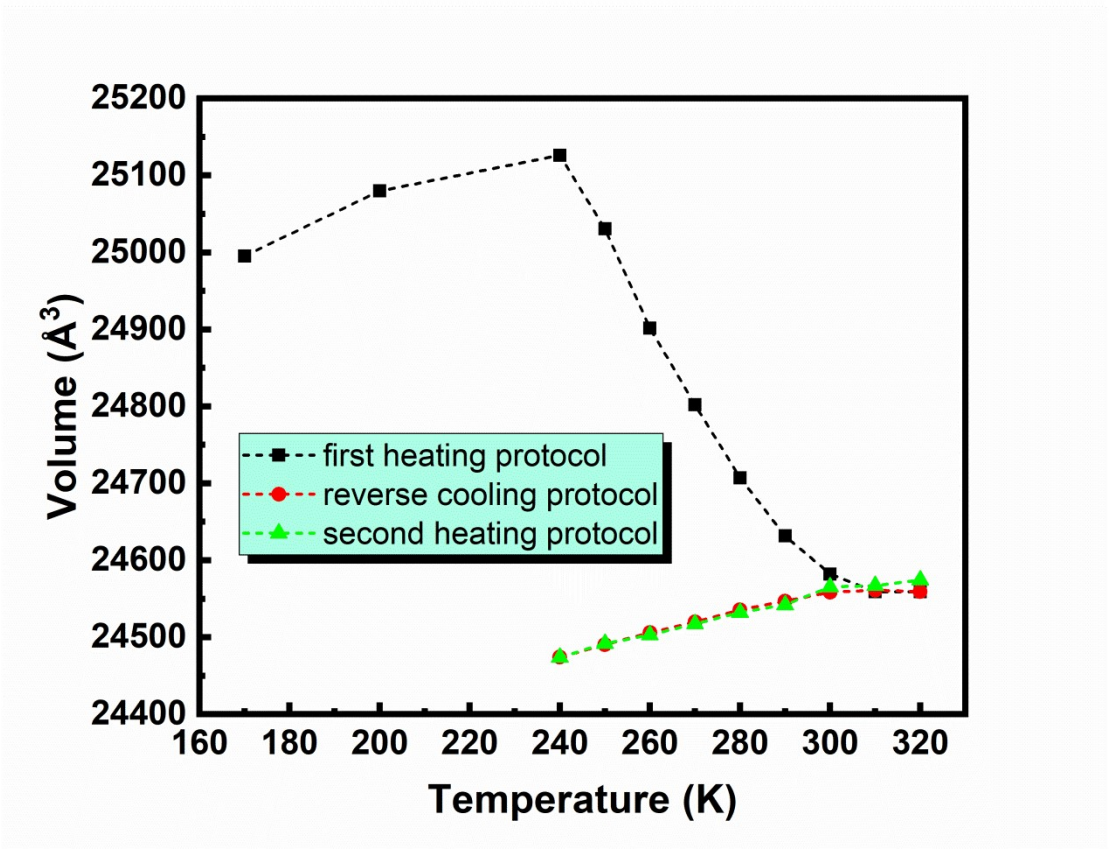

Fig. S25 Thermal response cycle test starting from 170 K: first heating protocol, 170 K-320 K; a following reverse cooling protocol, 320 K-240 K; second heating protocol, 240 K-320K.

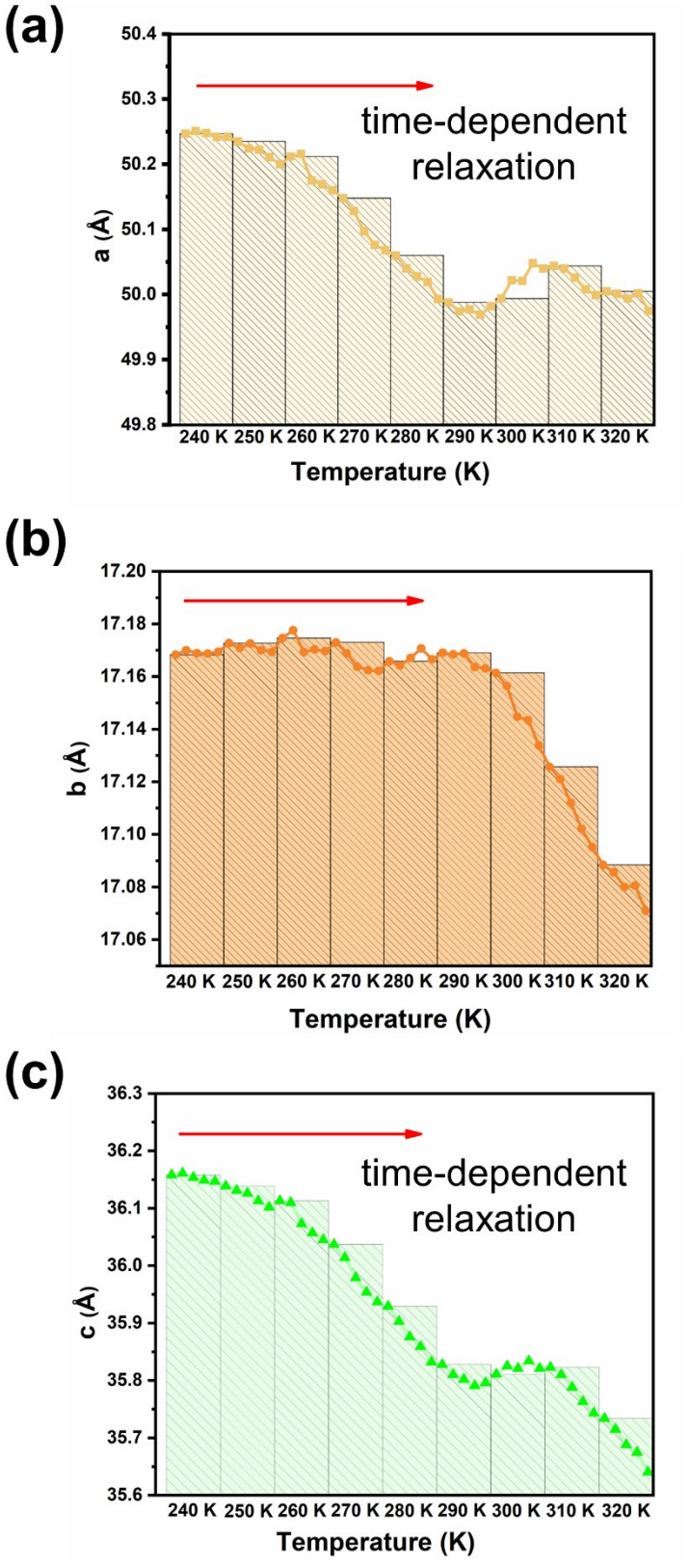

Fig. S26 Time-dependent relaxation process of different crystal axes recorded at different time intervals (10 min, 30 min, 60 min, 90 min and 120 min) at varying temperatures.

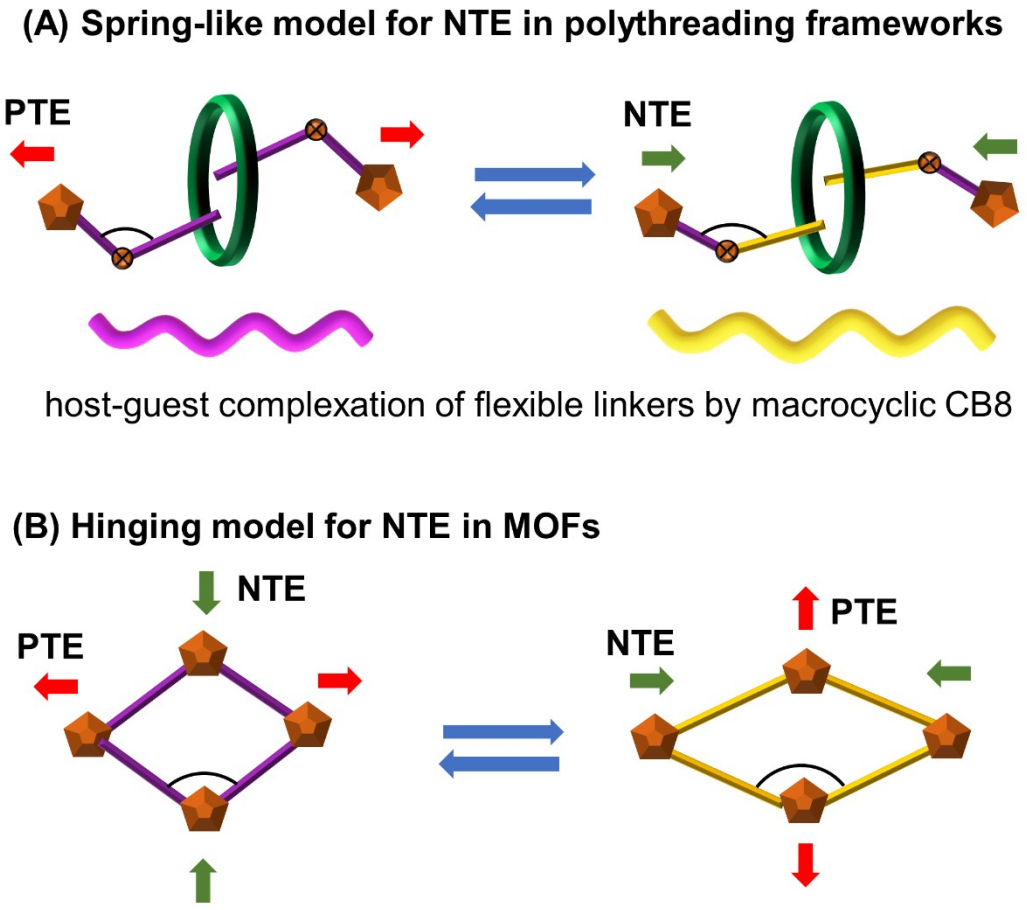

Fig. S27 A comparison between two different model for NTE: (A) spring-like model in polythreading frameworks; (B) hinging model in MOFs.

3. Supplementary Tables

Table S1. Crystallographic data and structure refinement results for $([Hbcbpy]_2@CB8)Cl_2$ and uranyl-organic polythreading framework, $U_3(bcbpy)_3(CB8)$.

	$([Hbcbpy]_2@CB8)Cl_2$	$U_3(bcbpy)_3(CB8)$
CCDC no.	2170894	2170893
formula	$C_{84}H_{77}N_{36}O_{20}$	$C_{204}H_{188}N_{76}O_{66}U_6$
fw	1910.81	6188.47
crystal system	monoclinic	monoclinic
space group	$P2_1/n$	$C2/c$
T, K	170	170
a, Å	14.2111(8)	50.174(2)
b, Å	20.6527(10)	17.1013(7)
c, Å	36.062(2)	36.5414(18)
α, degree	90	90
β, degree	98.644(2)	126.540(1)
γ, degree	90	90
V, Å^3	10463.7(10)	25191(2)
F (000)	3972.0	12096.0
Dc (g cm^{-3})	1.213	1.632
μ (mm^{-1})	0.091	3.936
R_{int}	0.0855	0.0341
R_1, wR_2 (I>=2σ (I))	0.0576, 0.1381	0.0455, 0.1001
R_1, wR_2 (all data)	0.0831, 0.1518	0.0630, 0.1133

Table S2. Typical U-O bond lengths for uranyl-organic polythreading framework, $U_3(bcbpy)_3(CB8)$.

Bond	Length (Å)	Bond	Length (Å)
U1-O1	1.777(4)	U3-O5	1.803(7)
U1-O2	1.780(4)	U3-O6	1.810(7)
U1-O7	1.777(4)	U3-O7	2.276(4)
U1-O8	1.780(4)	U3-O8	2.285(4)
U1-O10	2.398(4)	U3-O9	2.325(5)
U1-O12	2.429(4)	U3-O17	2.499(6)
U1-O16	2.455(4)	U3-O18	2.502(4)
U2-O3	1.765(4)		
U2-O4	1.788(5)		
U2-O7	2.235(4)		
U2-O9	2.318(4)		
U2-O13	2.352(4)		
U2-O14	2.529(4)		
U2-O15	2.481(4)		

Table S3. Typical O-O distances (D(O-O), Å, also see Fig. S11) of four different couples of opposite carbonyl groups on each portal of CB8 and the corresponding D_{max}/D_{min} for $([Hbcbpy]Cl)_2$@CB8 and $U_3(bcbpy)_3(CB8)$.

CB8 Type	D(O-O) (Å)	D_{max}/D_{min}
$([Hbcbpy]Cl)_2$@CB8	9.158(2)	1.153
	9.459(2)	
	10.562(3)	
	10.410(2)	
	8.796(2)	1.280
	9.904(2)	
	11.256(2)	
	10.137(2)	
$U_3(bcbpy)_3(CB8)$ -Type A	9.258(9)	1.146
	9.651(9)	
	10.614(11)	
	9.959(10)	
$U_3(bcbpy)_3(CB8)$ -Type B	9.384(7)	1.100
	9.837(7)	
	10.322(9)	
	10.102(9)	

Table S4. Lattice parameters extracted from the experimental VT-PXRD data in the range of 170 K to 320 K through profile fitting using the Pawley refinement.

T (K)	a (Å)	b (Å)	c (Å)	β (º)	V (Å^3)	R_{wp} (%)
170	49.3994	17.0386	35.3851	126.1621	24046	7.87
190	49.4817	17.0427	35.3886	126.1093	24110	11.91
210	49.6215	16.9616	35.6822	126.9593	23998	6.18
230	49.7815	17.1282	35.8340	126.9770	24409	7.02
240	49.7605	17.0041	35.8638	127.0325	24225	4.67
250	50.1704	17.1827	36.1745	127.1148	24868	5.67
260	50.2448	17.1706	36.4681	127.1170	25088	7.30
270	50.1803	17.1129	36.3010	127.0210	24889	6.19
280	49.9455	17.0470	36.0626	127.0206	24515	6.01
290	49.9413	17.0816	36.0064	127.2204	24460	5.63
300	49.6575	16.9660	35.7830	127.1110	24041	5.00
310	49.4606	16.8991	35.5922	127.0539	23742	5.23
320	49.7971	17.1142	35.8178	126.9594	24392	5.13

Table S5. Crystallographic data of $U_3(bcbpy)_3(CB8)$ within the temperature range from 170 K to 330 K.

T, K	**170**	**190**	**210**	**230**	**240**	**250**	**260**
CCDC no.	2170893	2170890	2170889	2170892	2170891	2170888	2170887
crystal system	monoclinic	monoclinic	monoclinic	monoclinic	monoclinic	monoclinic	monoclinic
space group	*C*2/c	*C*2/c	*C*2/c	*C*2/c	*C*2/c	*C*2/c	*C*2/c
V, Å^3	25191(2)	25204(2)	25314(9)	25349(7)	25382(8)	25454(9)	25506(8)
a, Å	50.174(2)	50.203(3)	50.309(9)	50.377(7)	50.392(8)	50.415(8)	50.442(7)
b, Å	17.1013(7)	17.1051(8)	17.123(3)	17.131(2)	17.139(3)	17.153(3)	17.173(2)
c, Å	36.5414(18)	36.545(2)	36.562(9)	36.574(8)	36.582(8)	36.605(9)	36.609(8)
β, degree	126.540(1)	126.570(2)	126.516(9)	126.572(7)	126.549(8)	126.479(10)	126.454(9)
D, g/cm^3	1.632	1.631	1.624	1.622	1.619	1.615	1.612
***T*, K**	**270**	**280**	**290**	**300**	**310**	**320**	**330**
CCDC no.	2170901	2170900	2170899	2170898	2170897	2170896	2170895
crystal system	monoclinic	monoclinic	monoclinic	monoclinic	monoclinic	monoclinic	monoclinic
space group	*C*2/c	*C*2/c	*C*2/c	*C*2/c	*C*2/c	*C*2/c	*C*2/c
V, Å^3	25291(13)	24839(8)	24641(9)	24560(8)	24614(10)	24664(11)	24770(12)
a, Å	50.361(12)	50.132(7)	49.985(8)	49.896(8)	49.939(10)	50.010(11)	50.078(12)
b, Å	17.160(4)	17.158(3)	17.153(3)	17.153(3)	17.159(3)	17.139(4)	17.124(4)
c, Å	36.437(13)	36.049(8)	35.852(9)	35.759(8)	35.770(10)	35.795(12)	35.793(13)
β, degree	126.564(12)	126.771(7)	126.717(9)	126.629(7)	126.581(9)	126.497(10)	126.195(13)
D, g/cm^3	1.625	1.655	1.668	1.673	1.670	1.667	1.659

Table S6. A comparison of volumetric coefficient α_V for NTE MOFs reported so far with that of $U_3(bcbpy)_3(CB8)$ in this work.

Compound	**α_V (10^{-6} K^{-1})**	**Temperature range (K)**	**Ref.**
$Cu_3(BTC)_2$ (HKUST-1)	-12.3	80-500	Wu et al., 2008[6]
$Zn_4O(BDC)_3$ (MOF-5)	-39.3	80-500	Lock et al., 2010[7]
$Cu_3(BTB)_2$ (MOF-14)	-26	3-400	Wu et al., 2014[8]
UiO-66(Hf)	-97	433-613	Cliffe et al., 2015[9]
$Zn_2(BDC)_2(dabco)$	-7.0	150-298	Kim et al., 2016[10]
MIL-68(In)	–12.3	125-600	Liu et al., 2018[11]
$Cu_3(BTC)_2$	−15.3	110-310	Schneider et al., 2019[12]
$TCNQ@Cu_3(BTC)_2$	-8.4	110-310	Schneider et al., 2019[12]
$Zn_8(SiO_4)(m\text{-}BDC)_6$	-4.4	100-475	Liu et al., 2019[13]
$Cd_2C_4O_4{\cdot}2H_2O$	-13.9	100-350	Liu et al., 2020[14]
Cu-TDPAT	-19.7	100-500	Asgari et al, 2021[15]
URCP1	-46.8	150-300	Li et al, 2021[16]
$U_3(bcbpy)_3(CB8)$	-962.9	260-300	This work

Table S7. Thermo-triggered variation of opening angles of three V-shaped bcbpy groups (ψ1, ψ2 and ψ3) in the hexanuclear uranyl unit within the whole range of 170-330 K

T (K)	ψ(degree)	ψ_2 (degree)
170	113.5(5)	73.6(4)
210	113.8(4)	74.9(3)
240	114.0(4)	76.0(3)
260	114.2(5)	76.4(3)
270	114.1(5)	77.1(4)
280	113.5(4)	78.5(3)
290	113.6(4)	79.5(3)
300	113.9(4)	80.2(3)
330	113.8(5)	82.7(4)

References

1. A. Day, A. P. Arnold, R. J. Blanch and B. Snushall, *J. Org. Chem.*, 2001, **66**, 8094-8100.
2. G. M. Sheldrick, *Acta Crystallogr. A*, 2008, **64**, 112-122.
3. G. M. Sheldrick, *Acta Crystallogr. A*, 2015, **71**, 3-8.
4. O. V. Dolomanov, L. J. Bourhis, R. J. Gildea, J. A. K. Howard and H. Puschmann, *J. Appl. Crystallogr.*, 2009, **42**, 339-341.
5. M. J. Cliffe and A. L. Goodwin, *J. Appl. Crystallogr.*, 2012, **45**, 1321-1329.
6. Y. Wu, A. Kobayashi, G. J. Halder, V. K. Peterson, K. W. Chapman, N. Lock, P. D. Southon and C. J. Kepert, *Angew. Chem. Int. Ed.*, 2008, **47**, 8929-8932.
7. N. Lock, Y. Wu, M. Christensen, L. J. Cameron, V. K. Peterson, A. J. Bridgeman, C. J. Kepert and B. B. Iversen, *J. Phys. Chem. C*, 2010, **114**, 16181-16186.
8. Y. Wu, V. K. Peterson, E. Luks, T. A. Darwish and C. J. Kepert, *Angew. Chem. Int. Ed.*, 2014, **53**, 5175-5178.
9. M. J. Cliffe, J. A. Hill, C. A. Murray, F. X. Coudert and A. L. Goodwin, *Phys. Chem. Chem. Phys.*, 2015, **17**, 11586-11592.
10. Y. Kim, R. Haldar, H. Kim, J. Koo and K. Kim, *Dalton Trans.*, 2016, **45**, 4187-4192.
11. Z. N. Liu, Q. Li, H. Zhu, K. Lin, J. X. Deng, J. Chen and X. R. Xing, *Chem. Commun.*, 2018, **54**, 5712-5715.
12. C. Schneider, D. Bodesheim, M. G. Ehrenreich, V. Crocella, J. Mink, R. A. Fischer, K. T. Butler and G. Kieslich, *J. Am. Chem. Soc.*, 2019, **141**, 10504-10509.
13. Z. N. Liu, X. X. Jiang, C. M. Wang, C. X. Liu, Z. S. Lin, J. X. Deng, J. Chen and X. R. Xing, *Inorg. Chem. Front.*, 2019, **6**, 1675-1679.
14. Z. N. Liu, R. Ma, J. X. Deng, J. Chen and X. R. Xing, *Chem. Mater.*, 2020, **32**, 2893-2898.
15. M. Asgari, I. Kochetygov, H. Abedini and W. L. Queen, *Nano Res.*, 2021, **14**, 404-410.
16. F. Z. Li, J. S. Geng, K. Q. Hu, L. W. Zeng, J. Y. Wang, X. H. Kong, N. Liu, Z. F. Chai, L. Mei and W. Q. Shi, *Chem. Eur. J.*, 2021, **27**, 8730-8736.